

Magnetism and electronic properties of BiFeO₃ under lower pressure

Hongjian Feng

*Department of Physics and Astronomy, University of Missouri, Columbia, MO
65211, USA*

Abstract

Ab initio calculations show an antiferromagnetic-ferromagnetic phase transition around 9-10 GPa and a magnetic anomaly at 12 GPa in BiFeO₃. The magnetic phase transition also involves a structural and insulator-metal transition. The G-type AFM configuration under pressure leads to an increase of the y component and decrease of the z component of the magnetization, which is caused by the splitting of the d_{z^2} orbital from doubly degenerate e_g states. Our results agree with recent experimental results.

Key words: G-type AFM structure;Phase transition;Dzyaloshinskii-Moriya interaction(DMI)

PACS: 75.30.Et,75.30.GW,71.15.Mb

1 Introduction

Multiferroic materials have more than two of ferroelectric/antiferroelectric, ferromagnetic/ antiferromagnetic, and even ferroelastic/ antiferroelastic ordering in same phase [1,2,3,4]. This feature makes them have potential applications in information storage, spintronics, and sensors. The study on BiFeO₃, a

Email address: fenghongjian@gmail.com, fengh@missouri.edu (Hongjian Feng).

multiferroic, which possess weak ferromagnetism and ferroelectric properties simultaneously at room temperature, has been recovered recently.[5,6,7]. It has long been known to be ferroelectric with a Curie temperature of about 1103 K and G-type antiferromagnetic(AFM) with a Néel temperature of 643 K. The large difference between the magnetic and ferroelectric ordering temperature makes the linear magnetoelectric coefficient smaller. Moreover,the $R3c$ space group permits a spiral spin structure in which the AFM axis rotates through the crystal with a long-wavelength period of 620\AA , which further reduces the observed G-type AFM magnetization. Fortunately, the decrease of magnetization can be compensated by doping in B-site of perovskites and fabricating thin film samples[8,9,10]. The ferroelectricity is produced by the Bi-6s stereochemically active lone pair , which can only occur if the cation ionic site have broken inversion symmetry, while the weak magnetism is mainly attributed to Fe^{3+} ions. The coupling between magnetic and ferroelectric parameter is weak because they are driven by different ionic sites, and this agrees with the fact of large difference between the Curie temperature and AFM Néel temperature. Through first-principles calculations, we have shown that the rotation of the oxygen octahedra(antiferrodistortive(AFD) distortion) couples with the weak ferromagnetism due to the Dzyaloshinskii-Moriya interaction(DMI), considering the spin-orbital(SO) coupling effect and the non-collinear spin configuration[11].

The study of BiFeO_3 under pressure should give us much insight in the understanding of the magnetoelectric coupling because it involves interesting structural and magnetic changes under pressure. Another metal-insulator transition and magnetic anomaly have already been reported recently[12,13]. Meanwhile, A. J. Hatt and coworkers performed the first principles calculations on strain induced phase transition of BiFeO_3 film on the (001)-oriented substrate[14,15]. An isosymmetric phase transition accompanying with dramatic structural change has been found. The two isosymmetric phases have the same space-group symmetry due to the constraints caused by coherence and epitaxy. The isosymmetric transition also indicates the coexistence of the rhombohedral and tetragonal phases. The rhombohedral film tends to be expanded with large compressive strain. And the lattice expansion can be accommodated by the increase of tetragonal domain. Further theoretical cal-

culations about the phase transition of BiFeO_3 need to be done to explain the detailed mechanism under pressure. We have performed first-principles calculations to investigate the magnetic and electronic properties of BiFeO_3 under lower pressure range corresponding to the experiments to shed light on the mechanism. The remainder of this article is structured as follows: In section 2, the computational details of our calculations are given. We discuss the results in section 3. Our conclusion are given in section 4.

2 Computational details

We performe calculations within the local spin density approximation(LSDA) to DFT using the ABINIT package[16,17]. The ion-electron interaction is modeled by the projector augmented wave (PAW) potentials [18,19] with energy cutoff of 500 eV. We treat Bi 5d, 6s, and 6p electrons, Fe 4s, 4p,and 3d electrons, and O 2s and 2p electrons as valence states. $10 \times 10 \times 10$ Monkhorst-Pack sampling of the Brillouin zone are used in calculations. LSDA+U method is introduced, where the strong coulomb repulsion between localized d states has been considered by adding a Hubbard-like term to the effective potential[20,21,22].

3 Results and discussion

3.1 FM behavior

According to the experimental results and previous calculations[13,23], we have constructed three structures, rhombohedral, monoclinic, and orthorhombic structures, with space group $R3c$, Cm , and $Pnma$, respectively. The lattice parameters are given in Table 1. The phase transition under pressure have been discussed elsewhere, and we suggest there exists a first-order phase transition from $R3c$ to Cm structure around 9-10 GPa, and gradually to pure $Pnma$ structure around 12 GPa which is close to the experimental values[13].We only report the magnetic and electronic behavior in this work. FM spin configuration for each structure are used to analyze the magnetization under pressure.

The FM magnetization are shown in Fig.1. One can see the spin value for the monoclinic structure is generally larger than the other two structures, and it exhibits a decrease of spin magnetization with increasing pressure and leads to a flat curve after passing 9-10 GPa. The monoclinic and rhombohedral structures both have the same spin value at all pressure range, indicating they have same structure dependent spin configuration. Moreover the phase transition between these two can be much easier than others. The transition between these two structures happens at 9-10 GPa. That between rhombohedral and orthorhombic structures take places at higher pressure of 12 GPa.

3.2 AFM-FM spin order transition

Meanwhile, for rhombohedral structure we set up three spin configurations, FM, AFM, and G-type AFM spin structures. The total energy per unit cell for different spin configuration have been calculated and shown in Fig. 2, as well as considering the on-site Coulomb interaction term, U . In LSDA+ U calculations, U and J are defined as

$$U = \frac{1}{(2l+1)^2} \sum_{m,m'} \langle m, m' | V_{ee} | m, m' \rangle = F^0, \quad (1)$$

$$J = \frac{1}{2l(2l+1)} \sum_{m \neq m', m'} \langle m, m' | V_{ee} | m, m' \rangle = \frac{F^2 + F^4}{14}, \quad (2)$$

where V_{ee} are the screened Coulomb interaction among the nl electrons. F^0 , F^2 , and F^4 are the radial Slater integrals for d electrons in Fe. It is apparent that there are intersection points between the FM and AFM energy curves. As pressure approaches the intersection points, both LSDA+ U and LSDA give lower AFM energy. However FM energy are much favorable after pressure exceeds the intersections, indicating an AFM-FM phase transition around the pressure value of 9-10 GPa. The LSDA+ U can produce relatively higher energy. On-site coulomb interaction, U is the energy needed to put two electrons in the same site. The value of U among the electrons in transition-metal d orbitals are one magnitude higher than the Stoner parameter. An appropriate band gap can be obtained in transition-metal oxides with properly choosing the U parameter. In our calculation we choose $U=2$ eV as it is rightly under the critical value to preclude the DMI in G-type AFM spin configuration,

where the Fe ions are arranged antiferromagnetically along x direction[24]. We take into account the non-collinear spin structure and spin-orbital(SO) interaction in G-type configuration. One can see that the G-type spin structure leads to a lower energy comparing with the FM and AFM one within LSDA+U scheme. Except the anomaly around the first transition pressure of 9-10 GPa, there is another one around 12 GPa. The relaxation results show the structure is changed into an orthorhombic phase at this pressure.

3.3 Exchange interaction

Consideration the Heisenberg model,

$$\Delta E = -1/2 \sum_{i,j} J_{i,j} \mathbf{S}_i \cdot \mathbf{S}_j, \quad (3)$$

for FM spin configuration, the total energy involving the spin exchange interaction can be written as,

$$E_{FM} = E_t - Z_c J_z S^2, \quad (4)$$

where E_t is the total energy without the spin, Z_c is the number of nearest neighboring Fe ions, and J_z is the exchange integral. While the AFM total energy has the form,

$$E_{AFM} = E_t + Z_c J_z S^2. \quad (5)$$

Therefore, we can determine the exchange parameters from the energy difference between different spin configurations. We set up the FM structure with spin direction along z axis while the G-type along x direction. From Fig. 3, it is obvious that $R\bar{3}c$ space group tends to produce a much favorable G-type structure. LSDA+U gives lower AFM exchange integral than LSDA. It is worth pointing out again that the anomaly takes place around the critical pressure value. Exchange integral even lies in the same level in these two schemes. G-type structure has lower exchange interaction under the whole pressure range. Two anomalies can be found at 9 and 12 GPa, respectively. It is consistent with energy calculations. When pressure exceeds the critical

value, AFM exchange integral is changing into a positive value where it applies to FM spin configuration. This shows the AFM-FM transition occurs at the critical pressure accompanying with the structural phase transition which agrees well with the previous total energy calculations. The phase graph under pressure is shown in Fig. 4. We suggest the rhombohedral structure maintains before the critical pressure value of 9 GPa. A combination of these three structures exist between 9 and 12 GPa, accompanying with an AFM-FM spin transition. A pure orthorhombic phase will be found after 12 GPa while the FM spin structure remains.

3.4 G-type AFM vectors

In G-type spin structure, we take into account the non-collinear and SO coupling effect. The AFM vectors under pressure are reported in Fig. 5. It is apparent that the AFM spin in x direction cancel out and a resultant magnetization along y and z direction can be obtained due to the DMI. DMI is caused by the interaction of neighboring Fe sites which can be described by

$$E_{Fe1,Fe2}^{(2)} = \mathbf{J}_{Fe1,Fe2}^{(2)}(\mathbf{S}_1 \cdot \mathbf{S}_2) + \mathbf{D}_{Fe1,Fe2}^{(2)}(\mathbf{S}_1 \times \mathbf{S}_2) + \mathbf{S}(R) \cdot \Gamma_{Fe1,Fe2}^{(2)} \cdot \mathbf{S}_2, \quad (6)$$

in the second order perturbation calculation[25,26]. The first term on the right hand side of the Eq. (6) corresponds to the usual isotropic superexchange interaction, and the second term is the DMI. The Hamiltonian for the system reads,

$$H_{BiFeO_3} = -2 \sum_{\langle 1i,2j \rangle} \mathbf{J}_{1i,2j} \mathbf{S}_{1i} \cdot \mathbf{S}_{2j} + \sum_{\langle 1i,2j \rangle} \mathbf{D}_{1i,2j} \mathbf{S}_{1i} \times \mathbf{S}_{2j}. \quad (7)$$

The first term is the symmetric superexchange, and the second one is the antisymmetric DMI contribution. $\mathbf{J}_{1i,2j}$ is a constant similar to the exchange interaction. \mathbf{D} is the DMI constant and determined by the sense of rotation of the neighboring oxygen octahedra. \mathbf{D} reads by the second order perturbation

in the case of one electron per ion

$$\mathbf{D}_{Fe1,Fe2}^{(2)} = (4i/U)[b_{nn'}(Fe1-Fe2)C_{n'n}(Fe2-Fe1)-C_{nn'}(Fe1-Fe2)b_{n'n}(Fe2-Fe1)], \quad (8)$$

where U is the energy required to transfer one electron from one site to its nearest neighbor, a parameter similar to on-site Coulomb interaction in our *Ab initio* computation, and inversely proportional to \mathbf{D} . The spin value along z direction is depressed after pressure exceeds the critical value while spin magnetization along y direction has the opposite trend and increases with pressure increasing. Firstly, the net magnetization has components along z and y direction simultaneously and deviate away from the z direction as pressure exceeds 12 GPa, resulting in zero component along z , while that along y direction increases and maintains a constant value after 12 GPa. The magnetization per unit cell is calculated based on the LSDA+U method and it is underestimated in this way. Therefore greater value is expected in LSDA calculations[24].

3.5 Electronic properties

In order to shed light on the electronic properties under pressure unambiguously, the total density of states(DOS) before and after exerting pressure are given in Fig. 6. The orbital resolved DOS(ODOS) for Fe 3d orbitals are given in Fig. 7 and Fig. 8, respectively. From Fig. 6, it can be seen that a semiconducting band gap of 1.7 eV is produced within LSDA+U while the band gap vanishes under pressure of 12 GPa, suggesting an obvious insulator-metal (IM) transition. The IM transition is mainly caused by the shift of the states of Fe 3d electrons in the vicinity of fermi energy. The finite DOS of these electrons cut through the fermi level and form a FM spin structure under 12 GPa. From Fig. 7, one can see all up-spin electrons are occupied and down-spin electrons are in conduction band. While almost all up and down spin states are partially filled under pressure in Fig. 8. Three-fold degenerate states t_{2g} coming from d_{xy} , d_{yz} , and d_{xz} orbitals remain degenerate, while d_{z^2} orbital splits from the two-fold degenerate states e_g . It is this orbital that makes e_g - e_g AFM interaction reduced. The splitting of the orbital under pressure is significant, suggesting the complete depression of AFM interaction and

the occurrence of FM spin structure. This is also the reason for the decrease of magnetization of G-type AFM structure along z direction under pressure. Meanwhile the down-spin Fe $3d$ states under pressure cut across the fermi energy and lead to the conducting behavior.

4 Conclusion

The total energy, magnetic and electronic properties of BiFeO₃ under pressure are calculated based on the LSDA and LSDA+U scheme. Results show two anomalies can be found at 9-10 GPa and 12 GPa, respectively. The first one is the critical pressure for first-order phase transition accompanying with AFM-FM transition. Meanwhile the behavior under critical pressure also involves an IM transition. The second one does not involve further magnetic transition but structural transitions. The magnetization of the G-type AFM spin structure in y direction increases while the z direction component decreases, which can be explained by the splitting of the d_{z^2} orbital from doubly degenerate e_g states.

References

- [1] M. Gajek, M. Bibes, and S. Fusil, Nature Mater. 6, 296 (2007).
- [2] Y. H. Chu, L. W. Martin, and M. B. Holcomb, Nature Mater. 7, 478 (2008).
- [3] H. Schmid, Ferroelectrics 162, 317 (1994).
- [4] M. Fiebig, J.Phys.D:Appl. Phys. 38, R123 (2005).
- [5] J. Wang, J. B. Neaton, H. Zheng, V. Nagarajan, S. B. Ogale, B. Liu, D. Viehland, V. Vaithyanathan, D. G. Schlom, U. V. Waghmare, N. A. Spaldin, K. M. Rabe, M. Wuttig, and R. Ramesh, Science 299,1719 (2003).
- [6] G. Catalan and J. F. Scott, Adv. Mater. 21, 2463 (2009).
- [7] Manoj K. Singh, S. Dussan, W. Prellier, and R. S. Katiyar, J. Mag. Mag. Mater. 321, 1706 (2009).

- [8] P. Baettig and N. A. Spaldin, *Appl. Phys. Lett.* 86, 012505 (2005).
- [9] S. Kamba, D. Nuzhnyy, R. Nechache, K. Zaveta, D. Niznansky, E. Santava, C. Harnagea, and A. Pignolet, *Phys. Rev. B* 77, 104111(2008)
- [10] H. Feng and F. Liu, *Phys. Lett. A* 372, 1904 (2008).
- [11] H. Feng and F. Liu, *Chin.Phys. Lett.* 25, 671 (2008).
- [12] Alexander G. Gavriliuk, Viktor V. Struzhkin, Igor S. Lyubutin, Sergey G. Ovchinnikov, Michael Y. Hu, and Paul Chow, *Phys. Rev.* 77, 155112 (2008)
- [13] R. Haumont, P. Bouvier, A. Pashkin, K. Rabia, S. Frank, B. Dkhil, W. A. Crichton, C. A. Kuntcher, and J. Kreisel, *Phys. Rev. B* 79, 184110 (2009)
- [14] O. E. Gonzalez Vazquez and Jorge Iniguez, *Phys. Rev. B* 79, 064102 (2009)
- [15] Alison J. Hatt, Nicola A. Spaldin, and Claude Ederer, *Phys. Rev. B* 81, 054109 (2010)
- [16] The ABINIT code is a common project of the Universite Catholique de Louvain, Corning, Inc., and other contributors(URL <http://www.abinit.org>).
- [17] X. Gonze, J.-M. Beuken , R. Caracas, F. Detraux, M. Fuchs, G.-M. Rignanes, F. Jollet, M. Torrent, A. Roy, M. Mikami, P. Ghosez, J.-Y. Raty , and D. C. Alan, *Comp. Mater. Sci.* 25, 478 (2002).
- [18] P. E. Blochl, *Phys. Rev. B* 50, 17953 (1994).
- [19] G. Kresse and D. Joubert, *Phys. Rev. B* 59, 1758 (1999).
- [20] V. I. Anisimov, J. Zaane, and O. K. Andersen, *Phys. Rev. B* 44, 943 (1991).
- [21] V. I. Anisimov, I. V. Solovyev, and M. A. Korotin, *Phys. Rev. B* 48, 16929 (1993).
- [22] V. I. Anisimov, F. Aryasetiawanz, and A. I. Lichtenstein, *J. Phys.: Condens. Matter.* 9, 767 (1997).
- [23] P. Ravindran, R. Vidya, A. Kjekshun, and H. Fjellvag, *Phys. Rev. B* 74, 224412 (2006)
- [24] H. Feng, *J. Magn. Mater.* 322, 1765 (2010).
- [25] P. W. Anderson, *Phys. Rev.* 115, 2 (1959).
- [26] T. Moriya, *Phys. Rev. Lett.* 4, 228 (1960).

Table 1

Current used lattice parameters for rhombohedral, monoclinic, and orthorhombic structures

| | <i>R3c</i> | <i>Cm</i> | <i>Pnma</i> |
|--------------------|---------------------------|----------------------|---|
| a(Å) | 5.459 | 5.7900 | 5.5849 |
| b(Å) | | 5.6899 | 7.6597 |
| c(Å) | | 4.1739 | 5.3497 |
| α (°) | 60.36 | | |
| β (°) | | 91.99 | |
| V(Å ³) | 115.98 | 137.42 | 113.12 |
| Bi | (2a):0,0,0 | (2a):0.9376,0,0.0685 | (4c):0.0536,0.2500,0.9886 |
| Fe | (2a):0.2308,0.2308,0.2308 | (2a):0.5110,0,0.4961 | (4b):0,0,0.5 |
| O | (6b):0.5423,0.9428,0.3980 | (2a):0.5626,0,0,9489 | (4c):0.9750,0.2500,0.4060; (4b):0.7958,0.7603,0.4231 (8d):0.2000,0.9540,0.1945 |

Figure captions:

Fig.1 FM magnetization for three phases of BiFeO₃ under pressure.

Fig.2 The total energy as functions of pressures.

Fig.3 The exchange integrals for different spin structures as functions of pressure.

Fig. 4 The phase graph of BiFeO₃ under pressure.

Fig. 5 G-type AFM vectors variations with respect to pressure.

Fig. 6 Total DOS under ambient and transition pressure.

Fig. 7 ODOS for Fe d_{xy} , d_{yz} , d_{z^2} , d_{xz} , and $d_{x^2-y^2}$ orbitals under ambient pressure.

Fig. 8 ODOS for Fe d_{xy} , d_{yz} , d_{z^2} , d_{xz} , and $d_{x^2-y^2}$ orbitals under transition pressure.

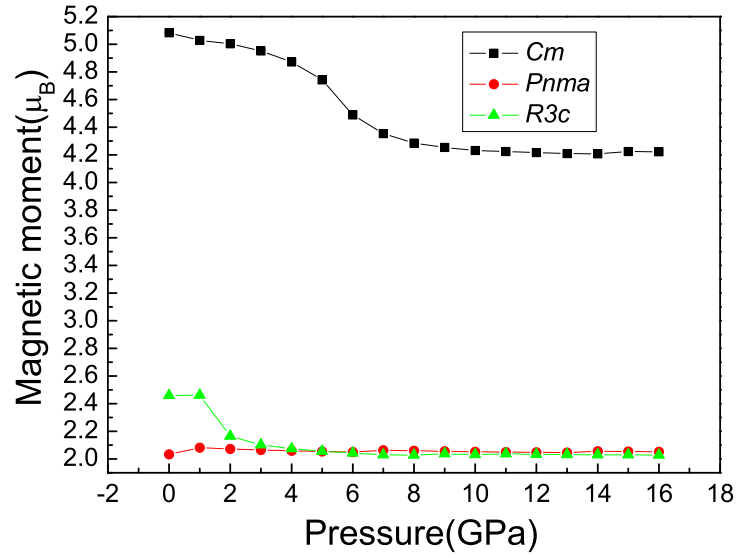


Fig. 1. FM magnetization for three phases of BiFeO₃ under pressure.

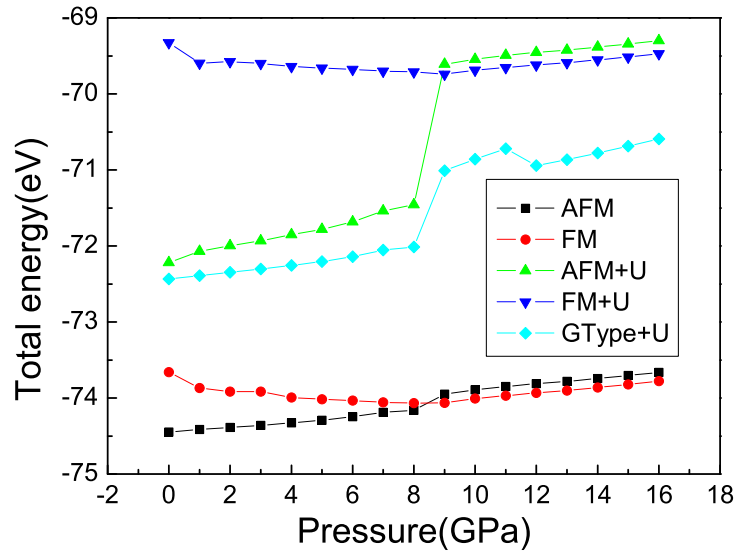


Fig. 2. The total energy as functions of pressures.

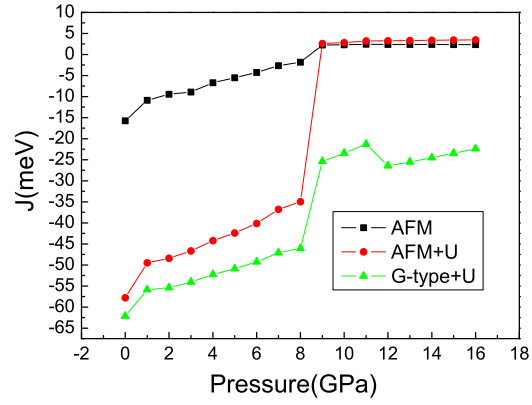


Fig. 3. The exchange integrals for different spin structures as functions of pressure.

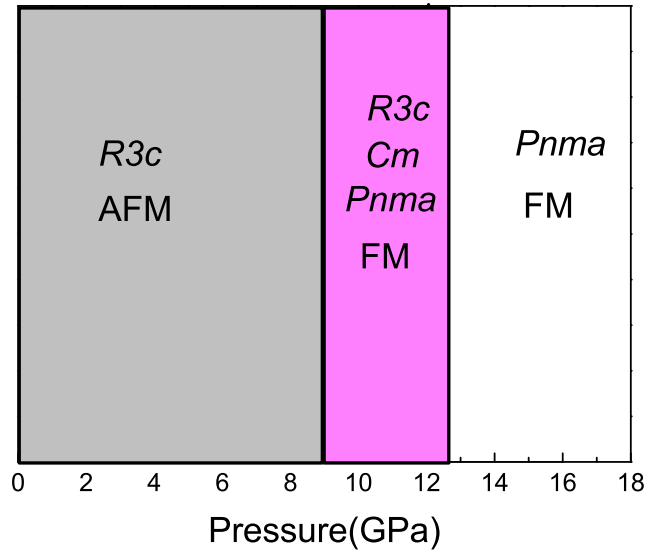


Fig. 4. The phase graph of BiFeO₃ under pressure.

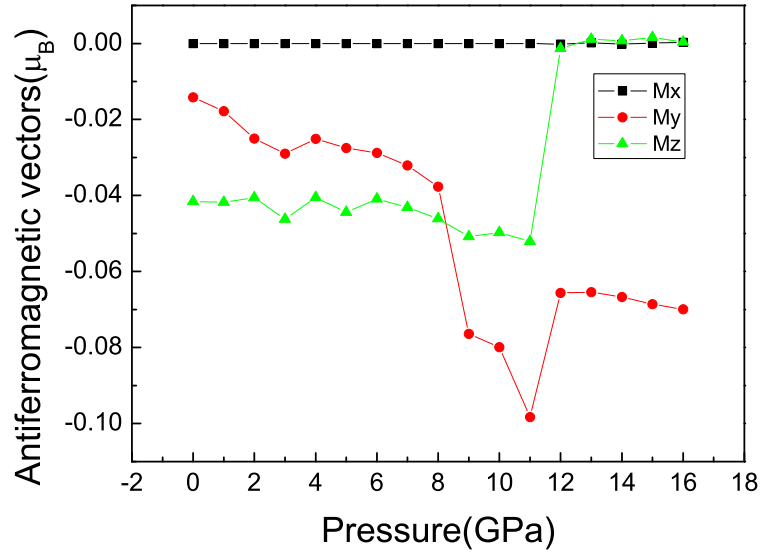


Fig. 5. G-type AFM vectors variations with respect to pressure.

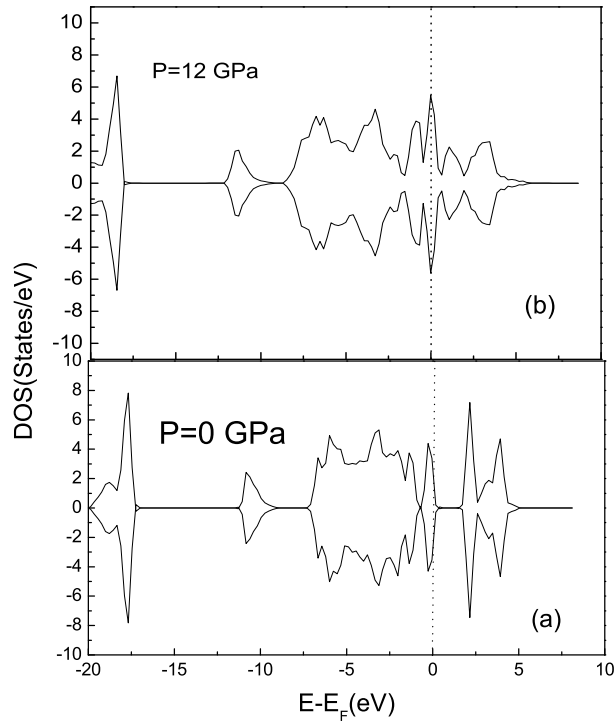


Fig. 6. Total DOS under ambient and transition pressure.

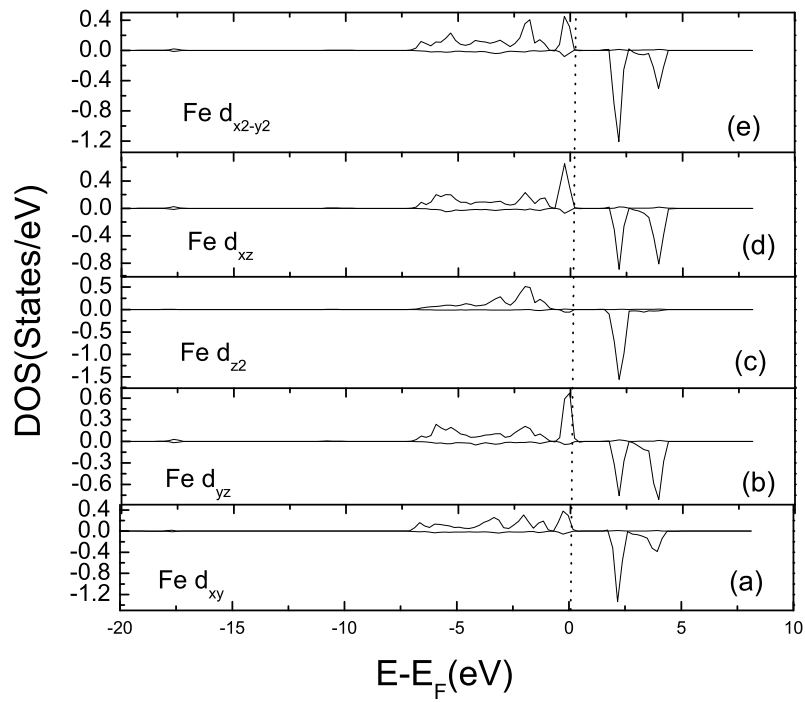


Fig. 7. ODOS for Fe d_{xy} , d_{yz} , d_{z^2} , d_{xz} , and $d_{x^2-y^2}$ orbitals under ambient pressure.

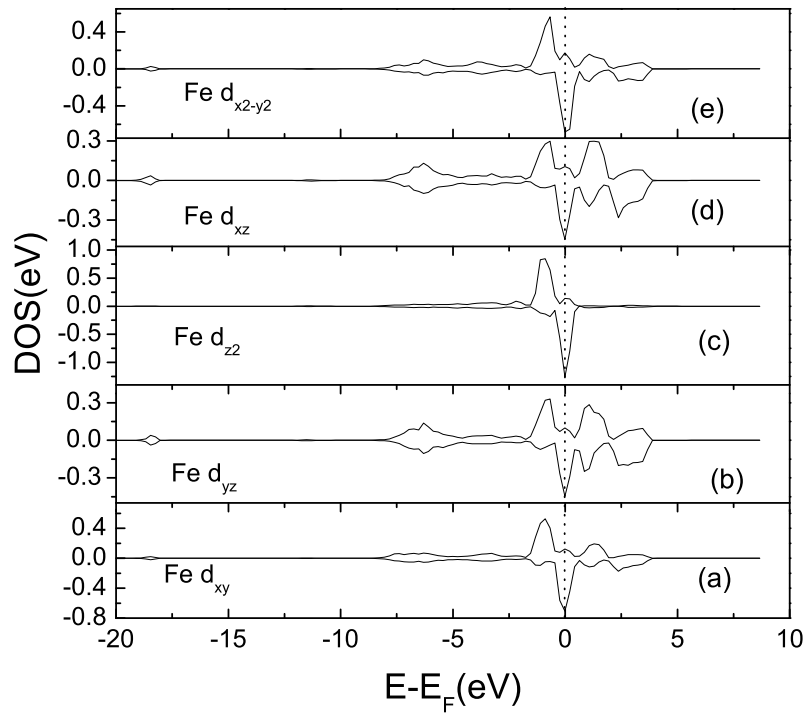


Fig. 8. ODOS for Fe d_{xy} , d_{yz} , d_{z^2} , d_{xz} , and $d_{x^2-y^2}$ orbitals under transition pressure.